Pulsed electromagnetic fields potentiate bone marrow mesenchymal stem cell chondrogenesis by regulating the Wnt/β-catenin signaling pathway

Kangping Song[1,2,3], Jing Hu[1,2,3], Ming Yang[4], Yong Xia[1,2,3], Chengqi He[1,2,3], Yonghong Yang[1,2,3*] and Siyi Zhu[1,2,3*]

Abstract

Background Pulsed electromagnetic fields (PEMFs) show promise as a treatment for knee osteoarthritis (KOA) by reducing inflammation and promoting chondrogenic differentiation of bone marrow-derived mesenchymal stem cells (BMSCs).

Purpose To identify the efficacy window of PEMFs to induce BMSCs chondrogenic differentiation and explore the cellular mechanism under chondrogenesis of BMSCs in regular and inflammatory microenvironments.

Methods BMSCs were exposed to PEMFs (75 Hz, 1.6/2/3/3.8 mT) for 7 and 14 days. The histology, proliferation, migration and chondrogenesis of BMSCs were assessed to identify the optimal parameters. Using these optimal parameters, transcriptome analysis was performed to identify target genes and signaling pathways, validated through immunohistochemical assays, western blotting, and qRT-PCR, with or without the presence of IL-1β. The therapeutic effects of PEMFs and the effective cellular signaling pathways were evaluated in vivo.

Results BMSCs treated with 3 mT PEMFs showed the optimal chondrogenesis on day 7, indicated by increased expression of ACAN, COL2A, and SOX9, and decreased levels of MMP3 and MMP13 at both transcriptional and protein levels. The advantages of 3 mT PEMFs diminished in the 14-day culture groups. Transcriptome analysis identified sFRP3 as a key molecule targeted by PEMF treatment, which competitively inhibited Wnt/β-catenin signaling, regardless of IL-1β presence or duration of exposure. This inhibition of the Wnt/β-catenin pathway was also confirmed in a KOA mouse model following PEMF exposure.

Conclusions PEMFs at 75 Hz and 3 mT are optimal in inducing early-stage chondrogenic differentiation of BMSCs. The induction and chondroprotective effects of PEMFs are mediated by sFRP3 and Wnt/β-catenin signaling, irrespective of inflammatory conditions.

Keywords Osteoarthritis, Pulsed electromagnetic fields, Mesenchymal stem cells

*Correspondence:
Yonghong Yang
nicole308@126.com
Siyi Zhu
hxkfzsy@scu.edu.cn
Full list of author information is available at the end of the article

Introduction

Knee Osteoarthritis (KOA) is the most common form of osteoarthritis, characterized by the gradual loss of articular cartilage. Manifestations include osteophyte formation, subchondral bone remodeling, and synovial inflammation, which collectively impair joint function and lead to chronic pain [1, 2]. KOA is responsible for approximately 60.8% of the global disability burden associated with osteoarthritis [3]. Between 1990 and 2019, the global prevalence of KOA increased by 22.42%, affecting nearly 365 million individuals and resulting in 11.5 million Years Lived with Disability (YLD). This accounts for 1.33% of the global disease burden, ranking KOA as the fourth most disabling condition [4].

The pathogenesis of KOA is complex, involving not only "wear and tear" but also interactions between micro-environmental and genetic factors during joint deterioration. An imbalance between matrix anabolism and catabolism contributes to the degeneration of osteoarthritic cartilage [5]. Current KOA management predominantly relies on pharmaceutical agents for symptomatic relief from pain and inflammation or on costly surgical procedures [6]. However, addressing KOA pathophysiology to alleviate structural damage and prevent long-term disability offers a promising strategy for developing novel interventions. Recent evidence-based guidelines for managing KOA prioritize non-pharmacological interventions, such as exercise, therapeutic modalities, and regenerative approaches, over pharmaceuticals or surgical options [1, 6, 7]. These interventions, supported by accumulating evidence, may restore matrix metabolism homeostasis by targeting multiple inflammatory or bone remodeling signals [8].

Cell-based therapy and novel approaches using mesenchymal stromal cells (MSCs) are promising regenerative rehabilitation strategies that have shown clinical benefits such as pain relief, increased cartilage thickness, and improved function for patients with KOA. However, intra-articular stem cell injections are not yet approved as a routine therapy [5, 6]. Bone marrow-derived mesenchymal stem cells (BMSCs) play a crucial role in tissue regeneration due to their ability to differentiate into various cell types, including osteoblasts, chondrocytes, and adipocytes. This highlights their potential in addressing degenerative conditions across different tissues [5]. Inducing chondrogenic differentiation of BMSCs to repair cartilage defects represents a promising strategy for treating KOA [9, 10]. The effectiveness of this approach has been investigated in both animal and human models, showing that intra-articular implantation of BMSCs in KOA patients can alleviate symptoms, improve SF-12 scores, and regenerate articular cartilage as observed through MRI [11]. However, the behavior and differentiation of BMSCs are significantly influenced by their surrounding microenvironment. Proinflammatory cytokines can adversely affect BMSCs' differentiation capacity by altering cellular metabolic pathways, such as the NF-κB [12, 13] and Wnt/β-catenin pathways [14], leading to disrupted metabolic balance and increased cell apoptosis. Research indicates that the presence of IL-1β suppresses the expression of genes encoding anabolic growth factors like ACAN and TGFB3, resulting in reduced glycosaminoglycan synthesis [15]. Additionally, IL-1β hinders MSCs' chondrogenesis by markedly activating NF-κB pathways, complicating cell-based healing of articular cartilage defects in inflamed joints [16]. Modulating Wnt/β-catenin signaling can alleviate IL-1β-induced inflammation and downregulation of chondrogenic marker expression [17], offering a potential therapeutic avenue to enhance chondrogenesis in inflammatory environments.

Pulsed electromagnetic fields (PEMFs) are recognized as a safe and effective treatment for KOA. A recent meta-analysis assessing the effectiveness of PEMFs on symptoms and quality of life in KOA patients revealed significant benefits in pain and stiffness relief [18]. Our team's guideline recommends PEMFs as an adjunctive intervention for symptom control and functional improvement in KOA [6]. Biologically, PEMFs exhibit a protective effect on joint cartilage and subchondral trabecular bone [19–21]. They significantly reduce inflammation by decreasing the expression of interleukin-1 beta (IL-1β), which disrupts the anabolic and catabolic activities of chondrocytes and contributes to cartilage degradation [22]. Moreover, PEMFs promote chondrogenic differentiation of BMSCs, enhancing tissue repair and regeneration [23]. For example, PEMFs at 75 Hz and 1.8 mT have successfully induced the differentiation of umbilical cord-derived MSCs into cartilaginous tissue [24]. Similarly, PEMFs at 75 Hz and 1.5 mT have shown effective induction of chondrogenic differentiation in bovine MSCs, evidenced by increased expression of aggrecan and type II collagen mRNA and the synthesis of proteoglycans [25]. However, the effectiveness of PEMFs in modulating cellular responses varies depending on factors such as frequency, intensity, and duration of exposure. One study found that a single 10-minute session of 15 Hz, 2 mT PEMFs yielded optimal chondrogenic outcomes and increased extracellular matrix (ECM) deposition [26]. Conversely, another study using rabbit adipose-derived stem cells (ADSCs) indicated that 50 Hz, 1.6 mT PEMFs over 21 days were more effective in inducing chondrogenesis [27]. Contradictorily, 75 Hz PEMFs at 1 mT, 3 mT, and 5 mT intensities inhibited the cartilaginous phenotype of BMSCs and increased ECM degradation after a 4-week treatment [28]. These varying results suggest a need to identify a therapeutic window for optimal PEMFs treatment. Our prior research

comparing different PEMFs frequencies (75/50/8 Hz) on KOA progression found that 75 Hz PEMFs offered the optimal chondroprotective and anti-inflammatory effects [29]. However, the optimal PEMFs intensity to fully harness the regenerative potential of BMSCs remains unexplored. Additionally, further investigation into the cellular mechanisms by which PEMFs induce chondrogenic differentiation in BMSCs is necessary.

In this study, we aimed to investigate the efficacy window of PEMFs treatment as an adjunct therapy for BMSC-based cartilage engineering, with a particular focus on intensity parameters. Using the optimal PEMFs treatment parameters, we sought to uncover the biological mechanisms that drive the chondrogenesis effect. Additionally, we introduced an inflammatory environment to simulate KOA pathology and explored how inflammation modulates BMSCs chondrogenic differentiation and the cellular mechanisms following PEMFs exposure. This comprehensive approach was intended to clarify the intricate relationship between PEMFs, BMSCs chondrogenesis, and inflammation, ultimately supporting the application of PEMFs as an adjunct treatment for BMSC-based cartilage regeneration in KOA.

Materials and methods
Isolation and culture of rat BMSCs
Sprague Dawley rat (male, 4 weeks, 85–100 g) were purchased from Chengdu Dossy Experimental Animals Co., Ltd. All animal studies adhered to the ARRIVE guidelines (Version 2.0) [30] and were ethically approved by the Institutional Animal Care and Use Committee of West China Hospital, Sichuan University (IACUC permit number: 20,220,224,091).

The detailed method for cell isolation and culture has been previously reported by us and others [31, 32]. Briefly, primary rat BMSCs were isolated from the femurs and tibias of three-week-old SD rats post cervical dislocation. Sprague Dawley rat were sacrificed by cervical vertebral luxation after anesthetization and then transferred to 75% ethyl alcohol for a few minutes. The femur and tibia were removed using surgical scissors and surgical forceps. Residual muscle and fascia were removed as much as possible before the bone marrow cavity was exposed. Then, the ends of the femur and tibia were cut with surgical scissors. The bone marrow cavity was flushed with αMEM (Biological Industries) supplemented with 10% FBS (Gibco) and 1% P/S (Gibco), followed by suspension culture at 37 °C in 5% CO_2. After 48 h, nonadherent cells were removed, and fresh complete medium was introduced, with subsequent medium changes every two days. Upon reaching 80–90% confluence, the cells were trypsinized and passaged at a 1:3 ratio. BMSCs from the third passage (P3 cells) were then used for subsequent experiments, and their morphology was observed.

Identification and differentiation of BMSCs
To assess BMSC purity [33], flow cytometry was used. P3 BMSCs were harvested, washed with 2% FBS staining buffer (2% FBS, BD Bioscience), and incubated with anti-rat CD34 (1:200, Biorbyt), CD44 (1:200, BD Pharmingen), CD45 (1:200, BD Pharmingen), and CD90.2 (1:200, BD Pharmingen) for 30 min in darkness. After being resuspended in 1 mL staining buffer and centrifuged at $800 \times g$ for 5 min, a total of 5×10^5 cells were measured via a flow cytometer (BD LSRFortessa, USA) and analyzed using FlowJo v10.4 software (Tree Star, USA).

For differentiation induction, P3 BMSCs were cultured in 12-well plates for osteogenesis and adipogenesis and in 3D pellet cultures for chondrogenesis. Induction media was replaced every three days according to the manufacturer's instructions. Alizarin red (Cyagen Biosciences Inc., China), Alcian blue (iCell Bioscience Inc., China), and Oil red (Cyagen Biosciences Inc., China) staining were performed on days 7, 14, and 21 to assess three-lineage differentiation.

PEMFs exposure system in vitro and in vivo
The PEMFs devices used in both in vitro and in vivo experiments were custom designed and manufactured through collaboration with the School of Mechanical Engineering of Sichuan University. Each device includes an adjustable regulated power supply, a signal generator, signal amplification, and Helmholtz coils. To prevent interference with magnetic fields, all components within the coils, such as flat stages, tube racks, and mouse cages, are made of plastic. The size of the in vitro coil was tailored to fit the cell incubator, and rigorous tests were conducted to ensure consistent PEMFs exposure intensity (Supplementary Fig. 2A). Graphical models of the PEMFs device and waveform sketches are provided (Supplementary Fig. 2B-C).

PEMFs treatment
We have proven a set of PEMFs parameters of frequency with osteoarthritis protective effects [19, 29, 34, 35]; therefore, intensity (unit, milli Tesla, mT) was the desired variable to be explored here. To screen the optimal PEMFs intensity, the flux intensity varied between 1.6 mT and 3.8 mT. Samples in both in vitro and in vivo experiments were exposed to spatially homogeneous, time-varying electromagnetic fields one hour per day, consisting of a square waveform of 75 Hz (burst width, 13.3 ms, no pulse-off duration) (Supplementary Fig. 3A - C). For treatment duration, animal models were exposed to PEMFs with the identified intensity for one month, while 7- and 14-day durations were designed for in vitro experiments.

BMSCs proliferation and migration analysis

P3 BMSCs were divided into five groups: (1) control (αMEM complete medium, with or without fetal bovine serum (FBS)), (2) 1.6 mT PEMFs, (3) 2 mT PEMFs, (4) 3 mT PEMFs, and (5) 3.8 mT PEMFs. Groups (2) to (5) were cultured with chondrogenic medium. For the control group, FBS was included in the proliferation experiments to provide basic nutritional support for cell growth. However, FBS was excluded during migration analysis to prevent its influence on scratch line measurement and transwell cell counts, which could be affected by cell proliferation. The setup for the other PEMF groups was consistent with the control group in the corresponding experiments.

To assess BMSCs proliferation in response to PEMFs, a Cell Counting Kit-8 (CCK-8) assay was conducted. BMSCs were seeded at a density of 1×10^4 cells per well in 96-well plates with complete medium. Following daily PEMFs exposure, CCK-8 solution was added according to the manufacturer's instructions (Yoshi, China). The absorbance was measured at 450 nm after a one-hour incubation.

To evaluate how PEMFs affect BMSCs migration, both scratch healing test and Transwell experiment (pore size, 8 μm, Millipore, USA) were employed. A total of 1×10^6 cells were grown to full confluence for the scratch healing test in 12-well plates. After creating a baseline scratch, the wells were washed with PBS, and serum-free αMEM medium was added. The distances between scratch borders were recorded to calculate the migration rate after 24-hour and 48-hour PEMFs exposure. In the Transwell experiment, 2×10^4 cells were seeded in the upper chambers of 24-well plates, while the lower chambers were filled with 500 μL of complete medium (containing 10% FBS). After 24–48 h of PEMFs exposure, the remaining cells in the upper chambers were removed, and the migrated cells were fixed with 4% paraformaldehyde for 10 min and stained with crystal violet (Beyotime, China) for 30 min. ImageJ software (v1.51, NIH, USA) was used to count the number of stained cells in three randomly selected fields per group.

Chondrogenic differentiation

To evaluate the impact of PEMFs intensities on chondrogenesis, P3 BMSCs were categorized into six groups: (1) control (αMEM complete medium, with FBS), (2) 0 mT, (3) 1.6 mT PEMFs, (4) 2 mT PEMFs, (5) 3 mT PEMFs, and (6) 3.8 mT PEMFs. Cells in groups (2) to (6) were cultured in chondrogenic medium and harvested on days 7 and 14 for assessment of cartilage-specific matrix proteins. Pellets were stained with Alcian blue and Safranin-O (Solarbio, China) to detect cartilage proteoglycan deposition following the manufacturer's protocols.

Histology and immunohistochemical assay

HE staining was conducted for histological analysis. AGGRECAN was used for immunohistochemistry (IHC) to confirm protein levels, the steps of which were performed according to the immunohistochemical protocol [36, 37]. Cell pellets were collected, fixed in 4% paraformaldehyde, decalcified, dehydrated and embedded in paraffin. Cell Sect. (4 μm) were cut and deparaffinized with xylene and rehydrated through an ethanol series, followed by treatment with 3% H_2O_2 and citrate buffer. Sections were then blocked with 10% normal goat serum for 1 h and incubated overnight at 4 °C with primary antibody (anti-ACAN, 1:100, Huabio, Cat# ET1704-57). followed by horseradish peroxidase-conjugated secondary antibodies (1:200, Bioss Cat# bs-0295D-HRP). Visualization was performed using DAB solution (Servicebio, China), followed by counterstaining with hematoxylin. Knee joint samples were prepared into 5-μm sections, and the primary antibodies included anti-ACAN (1:200, Abcam Cat# ab3778), COL2A (1:500, Proteintech Cat# 28459-1-AP), SOX9 (1:100, Huabio Cat# ET1611-56), MMP13 (1:200, Abcam Cat# Ab39012), ADAMTS4 (1:100, Abcam Cat# Ab185722), Wnt3a (1:400; Novus Cat# NBP1-74183), β-catenin (1:100; Novus Cat# NBP1-32239), and IL-1β (1:100, Bioss Cat# BS0812R).

Western blot analysis

Six pellets from each group were collected on day 7 and day 14 postinduction. Whole-cell extracts were lysed in RIPA buffer (Beyotime, China). Protein samples were separated by electrophoresis on SDS−PAGE gels and transferred to polyvinylidene fluoride (PVDF) membranes. The membranes were blocked with 5% nonfat milk and incubated overnight at 4 °C with specific primary antibodies. Subsequently, the PVDF membranes were washed and incubated with secondary antibodies. Immunoreactivity was detected using a chemiluminescence imager (Bio-Rad, USA). The commercial antibodies used included ACAN (Novus Cat# NB600-504), COL2A (Proteintech Cat# 28459-1-AP), SOX9 (Huabio Cat# ET1611-56), MMP3 (Huabio Cat# ET1705-98), MMP13 (Novus Cat# NBP2-45887), p65 (Cell Signaling Technology Cat# 8242), pp65 (Cell Signaling Technology Cat# 3033), STAT3 (Cell Signaling Technology Cat# 4904), p-STAT3 (Cell Signaling Technology Cat# 9145), β-catenin (Huabio Cat# ET1601-5), sFRP3 (Santa Cruz Cat# sc-514,350), β-actin (Huabio Cat# M1210-2), HRP-conjugated goat anti-rabbit IgG (Huabio Cat# HA1001), and HRP-conjugated goat anti-mouse IgG (Huabio Cat# HA1006). The diluted ratios for primary and secondary antibodies were 1:1000 and 1:5000, respectively. ImageJ software (v1.51, NIH, USA) was employed to quantify the gray values of the images. Briefly, the steps were

Song *et al. Journal of Translational Medicine*   (2024) 22:741

Page 5 of 19

performed according to the protocol of Western blot [38, 39].

Quantitative reverse-transcription PCR (qRT–PCR)

Ten pellets were collected from each group and homogenized in 300 μL TRIzol reagent (TaKaRa Cat#9109, Japan). Total RNA was extracted from the pellets and quantified using a NanoDrop 2000 spectrophotometer (Thermo Scientific, Waltham, USA). Complementary DNA was synthesized via reverse transcription using Hifair cDNA Synthesis SuperMix (Yeasen Biotechnology, China). qRT–PCR was performed using SYBR Green Master Mix (Vazyme Biotech, China) on a QuanStudio 3 (Applied Biosystems, CA) according to the manufacturer's protocol. Expression levels were normalized to β-actin. See Supplementary Table 1 for the primer sequences utilized.

Immunofluorescence staining

Sections for immunofluorescence (IF) were processed as described in the IHC assay and then incubated with the following primary antibodies overnight to evaluate protein expression levels: ACAN (1:200, Novusbio Cat# NB600-504), COL2A (1:100, Huabio Cat# ET1611-56) and SOX9 (1:200, Huabio Cat# ET1611-56). The next day, the sections were incubated with goat anti-rabbit IgG H&L (1:500, Abcam Cat# ab150077, UK) or goat anti-mouse IgG H&L (1:500, Abcam Cat# ab150115, UK) secondary fluorescent antibodies. Nuclei were counterstained with DAPI staining solution at room temperature for 10 min. Fluorescence signals were captured using a fluorescence upright microscope (Ni-E, Nikon, Japan). The fluorescence intensities of the acquired images were quantified using ImageJ software (v1.51, NIH, USA).

Transcriptome analysis

Total RNA was separated from 10 chondrogenic-induced pellets using a TRIzol reagent kit (Invitrogen Life Technologies, USA) following the manufacturer's protocol. The quality and integrity of the extracted RNA were assessed using RNase-free agarose gel electrophoresis and an Agilent 2100 Bioanalyzer (Agilent Technologies, Palo Alto, CA, USA), respectively. Eukaryotic mRNA was enriched and fragmented. The fragmented mRNA was subjected to reverse transcription to generate complementary DNA (cDNA), and libraries were then constructed. The resulting libraries were sequenced using the NovoSeq 6000 (Illumina) platform with paired-end 150 bp (PE150) reads. Gene set enrichment analysis (GSEA) was conducted to assess the enrichment of related genes in each comparison. The normalized enrichment score (NES) and nominal p value were utilized as metrics to quantify the level of enrichment. Enriched gene sets meeting the criteria of $|NES| > 1$ and

$p < 0.05$ were considered statistically significant. RNA-seq and bioinformatic analysis were performed on the platform by Suzhou PANOMIX Biomedical Tech Co., LTD.

Inflammation induction

With the identified optimal PEMFs intensity, P3 BMSCs were categorized into six groups: (1) control (αMEM complete medium), (2) control with IL-1β, (3) 0 mT PEMFs, (4) 0 mT PEMFs with IL-1β, (5) suitable parameter PEMFs exposure, and (6) suitable parameter PEMFs with IL-1β to evaluate the impact of inflammation on chondrogenesis. Cells from groups (2) to (6) were cultivated with chondrogenic medium, and 50 ng/ml IL-1β (MedChemExpress, Cat# HY-P7097, China) was applied to the corresponding groups to induce inflammation. Proteins indicating inflammation were assessed to verify the model, and chondrogenic-related proteins were evaluated again.

In vivo verification

Animal experiments on KOA mouse models were conducted to verify the identified optimal PEMFs parameters from in vitro experiments. C57BL/6 mice (male, 10–12 weeks, around 20 g) were used for animal experiments. Destabilization of the medial meniscus (DMM) surgery was performed on the right knee of mice for osteoarthritis (OA) induction as previously described [29]. Eighteen 10-week-old mice were randomly assigned into three groups (n=6 each): (1) sham DMM surgery (Control group), (2) DMM surgery (DMM group) and (3) PEMFs exposure post DMM surgery (PEMFs group). For the PEMF group, PEMFs exposure was initiated the day after DMM in the explored intensity from in vitro experiments, and other treatment parameters were meticulously aligned with the parameters utilized in the in vitro experiments. After 4 weeks of intervention, right knee joints were collected to complete IHC staining and histological analysis. Histological assessment of sagittal sections of the knee joints was conducted by two blinded observers following the Osteoarthritis Research Society International (OARSI) scoring system. Toluidine blue staining was conducted for histological analysis.

Statistical analysis

All data were analyzed with SPSS (v25.0, IBM, USA) and graphed with GraphPad Prism. Nominal data were expressed as the mean±SD, Student's t test (two groups) and one-way ANOVA (multiple groups), followed by Tukey's post hoc test. Ordinal data were analyzed using nonparametric Mann–Whitney U tests. P values less than 0.05 indicated statistical significance. The number of animal in each group was determined based on resource equation method [40].

Song *et al. Journal of Translational Medicine*   (2024) 22:741

Page 6 of 19

Results

Identification of BMSCs

The bone marrow was gently flushed with medium until the cavities displayed a faded appearance (Supplementary Fig. 1A). P3 BMSCs exhibited a spindle-like morphology (Supplementary Fig. 1B). Notably, the cell proliferation curve and the plotted curve exhibited a sigmoidal profile, indicating that P3 BMSCs transited into logarithmic growth on the second day and demonstrated a slight stagnation on the fifth day (Supplementary Fig. 1E). Alizarin Red, Oil Red and Alcian Blue staining confirmed the osteogenic, adipogenic and chondrogenic differentiation potential of P3 BMSCs (Supplementary Fig. 1C). Concurrently, cytometry results underscored the purity of P3 BMSCs, with surface marker percentages recorded as follows: CD34(negative rate: 98.1%), CD45 (negative rate: 96.6%), CD44 (positive rate: 99.2%) and CD90 (positive rate: 100%) (Supplementary Fig. 1D). These findings collectively confirm the cellular identity of the P3 BMSCs population.

PEMFs with specific parameters have no negative impact on BMSCs proliferation, and 3 mT PEMFs promote the migration of BMSCs

The potential detrimental effect of PEMFs on cell proliferation was determined by comparing the proliferation curves of the cells from different intervention groups. No difference was observed in the proliferation rate from various PEMFs exposures, indicating the safety of chosen PEMFs intensities for BMSCs (Fig. 1A).

Scratch healing and transwell experiments were employed to investigate the effects of PEMFs on BMSCs migration. In the transwell experiment, both 3 mT and 3.8 mT PEMFs promoted BMSC migration capacity at the 48-h time point when compared to the control group (Fig. 1E - G). However, the scratch healing experiment revealed the optimal effect of PEMFs at 3 mT intensity to promote BMSC migratory capacity at both 24 h and 48 h (Fig. 1B - D).

3 mT PEMFs promote chondrogenic differentiation of BMSCs in the early stage of chondrogenesis

Next, we compared BMSCs chondrogenic differentiation results after PEMFs treatments with multiple intensities. After 7 days of exposure, the pellet in the 3 mT group presented with the most intact morphology in HE staining and intense Safranin O and Alcian blue staining, which indicated a greater accumulation of glycosaminoglycans, proteoglycans and collagens and that 3 mT PEMFs might induce chondrocyte phenotypes of high quality. This optimal induction potential of 3 mT was further validated by a greater expression of AGGRECAN in IHC staining throughout the matrix (Fig. 2A). Western blot analysis further investigated the expression of chondrogenic-related proteins, and we found that PEMFs at 3 mT and 3.8 mT specifically upregulated the expression of ACAN and COL2A, and chondrogenic medium culture consistently upregulated SOX9, the biological initiator of chondrogenesis (Fig. 2B - E). However, as the exposure duration extended to 14 days, the initially robust chondrogenic phenotype exhibited a diminishing trend, and the superiority of 3 mT PEMFs also subsided (Fig. 3A). No discernible increase in anabolic-related factors was observed across the experimental groups (Fig. 3B - E). The weakening of anabolic-related molecules from day 7 to day 14 was further proven by IF staining (Fig. 4A – B and D - E).

We then explored how optimal PEMFs affect chondrogenesis at the transcriptional level with qPCR. On day 7, 3 mT PEMFs upregulated the expression of *aggrecan* and *col2a* and inhibited the expression of *mmp3* and *mmp13* (Fig. 4C), which confirmed the findings of Western blotting and IF staining and indicated a PEMFs-induced augmentation in chondrocyte-associated anabolic processes coupled with the simultaneous inhibition of the catabolic profile. After 14 days of exposure, 3 mT PEMFs still upregulated the expression of anabolic-related genes and suppressed the expression of catabolic genes. Nevertheless, the anabolic-promoting effect was less significant than the 7-day exposure period (Fig. 4F).

Among all intensities of interest, 3 mT emerged as the optimal parameter of PEMFs and potentially promoted BMSCs chondrogenic differentiation, particularly in the early chondrogenesis phase (day 7).

Frzb is the key factor in enhancing BMSCs chondrogenic differentiation with PEMFs exposure through modulating the Wnt/β-catenin signaling pathway

Next, we conducted transcriptome sequencing on BMSCs to unravel the underlying genetic mechanism responding to the optimal PEMFs exposure (Fig. 5A). Gene Ontology (GO) enrichment analysis of differentially expressed genes showed that 3 mT PEMFs modulated the chondrogenic process of BMSCs by affecting mechanisms such as collagen trimer, glycosaminoglycan binding, cartilage development, and response to external stimulus process only in day 7 samples, and the response to external stimulus process remained affected in day 14 samples (Fig. 5B). The GSEA analyses of the abovementioned enrichment genes are presented in Supplementary Fig. 4A-D. The dissimilarity of gene expression between 7-day and 14-day exposure aligned with evidence at the protein level that 3 mT PEMFs enhanced BMSCs chondrogenic differentiation only in the early phase.

Given that PEMFs mainly play a role in the early phase of induction, we primarily focused on the differential genes associated with day 7. Three genes (*frzb, plau, and sost*) were selected for further scrutiny from volcano
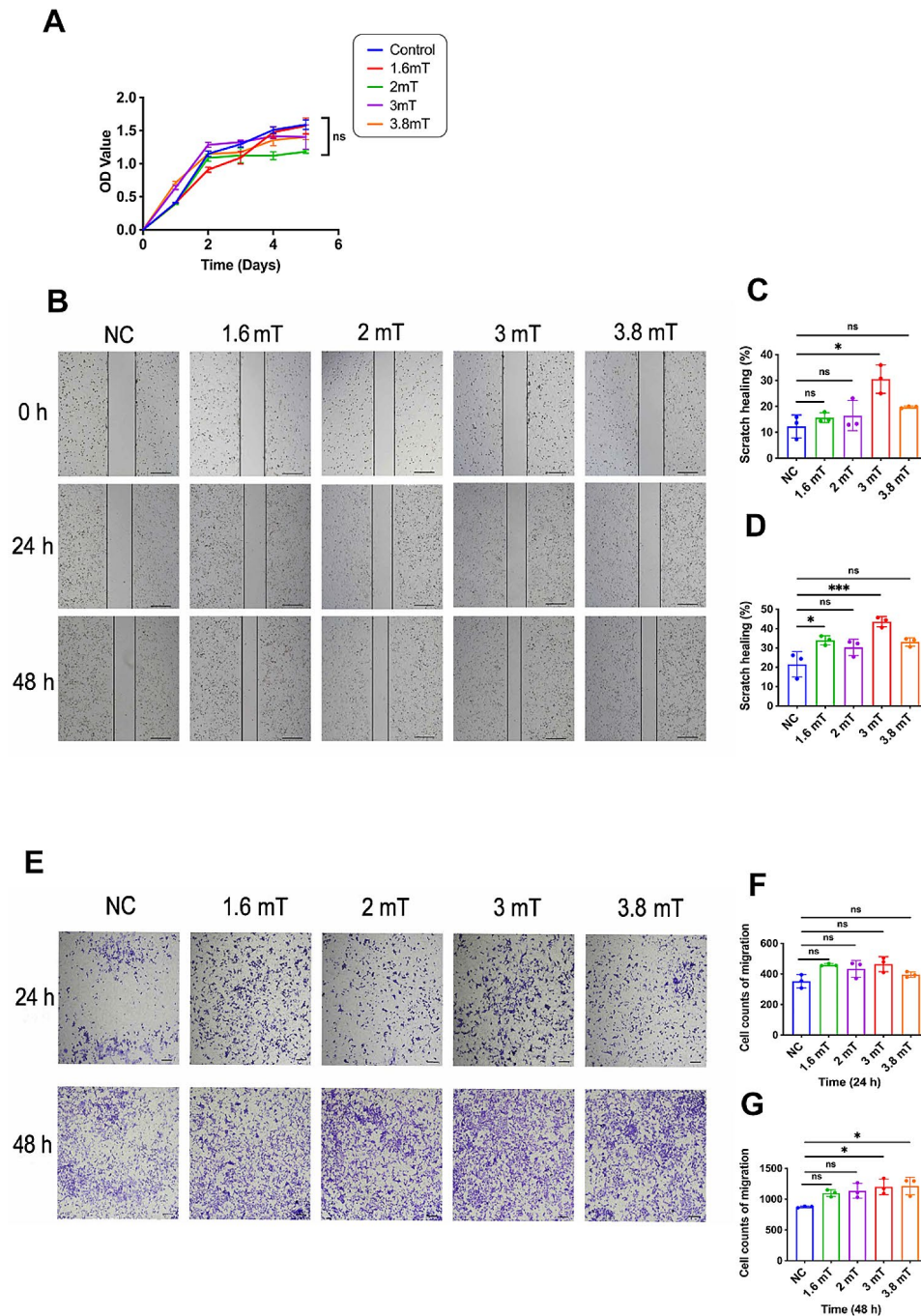
Fig. 1 PEMFs with specific parameters had no negative impact on BMSCs proliferation and 3 mT PEMFs promotes migration of BMSCs. **(A)** Proliferation curves of different intensities. **(B)** Migration of BMSCs was analyzed using scratch healing experiment and the borders were captured and the distance between borders were measured. **(C)** Quantification for relative distance in 24 h. **(D)** Quantification for relative distance in 48 h. **(E)** Migrated cells were also analyzed using a transwell cultured. The number of cells on the underside of the transwell filter after crystal violet staining were counted. **(F)** Quantification for cell counting in 24 h. **(G)** Quantification for cell counting in 48 h. ns, $p>0.05$; * $p<0.05$; ** $p<0.01$; *** $p<0.001$. Student's t test and one-way ANOVA were used for comparison between two groups and multiple groups, respectively

plots (Fig. 5C). With further corroboration of qPCR, only *frzb* was consistently upregulated by PEMFs (Fig. 5D - E). The sFRP3 protein is encoded by *frzb* and is known as an antagonist of the Wnt/β-catenin signaling pathway. Because sFPR3 competitively binds to Wnt ligands, it

effectively dampens Wnt/β-catenin pathway activation and inhibits the degradation of β-catenin. As a result, we evaluated the sFRP3 and β-catenin expression levels. The outcomes demonstrated that 3 mT PEMFs downregulated β-catenin only on day 7 but significantly increased
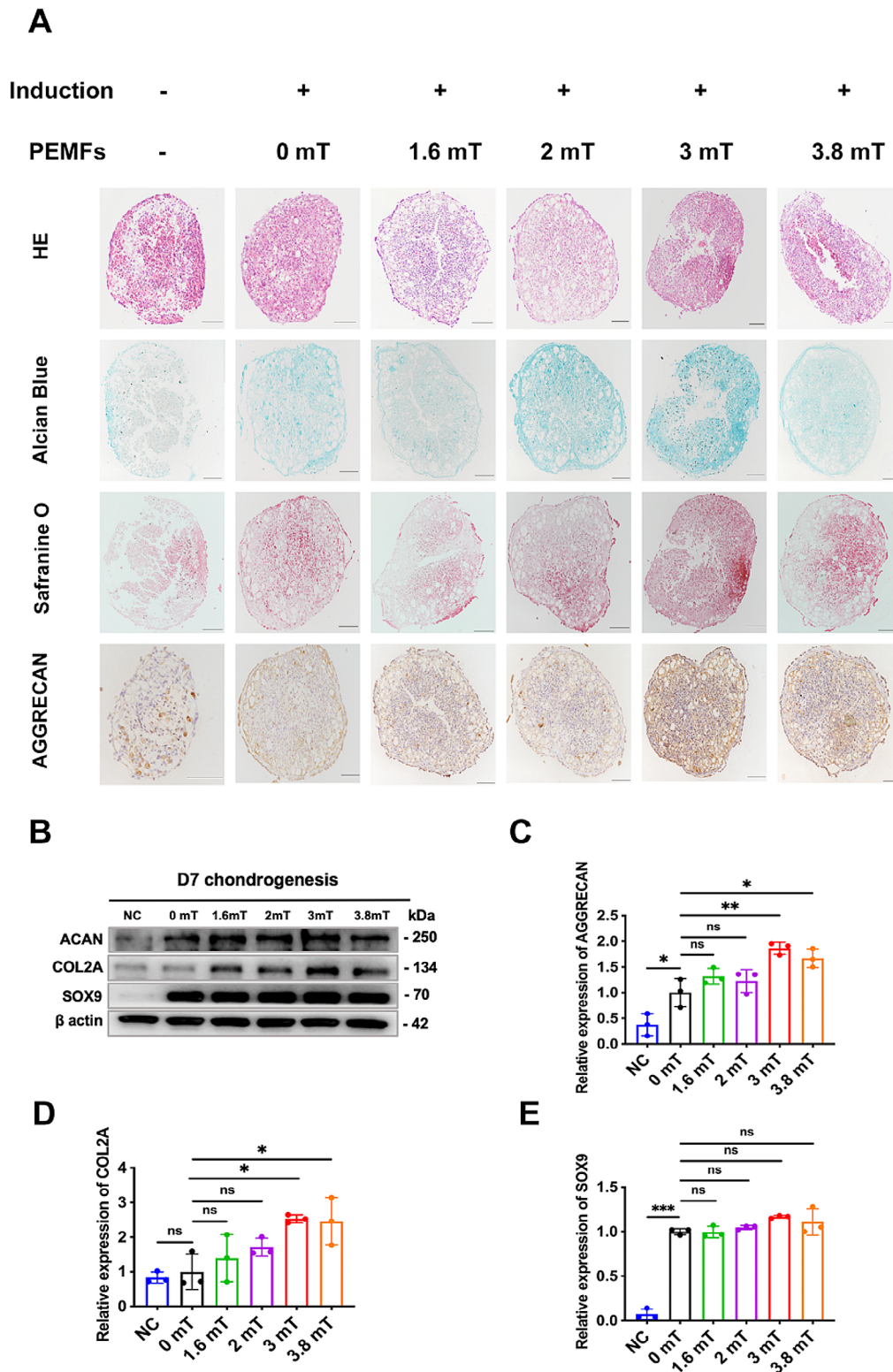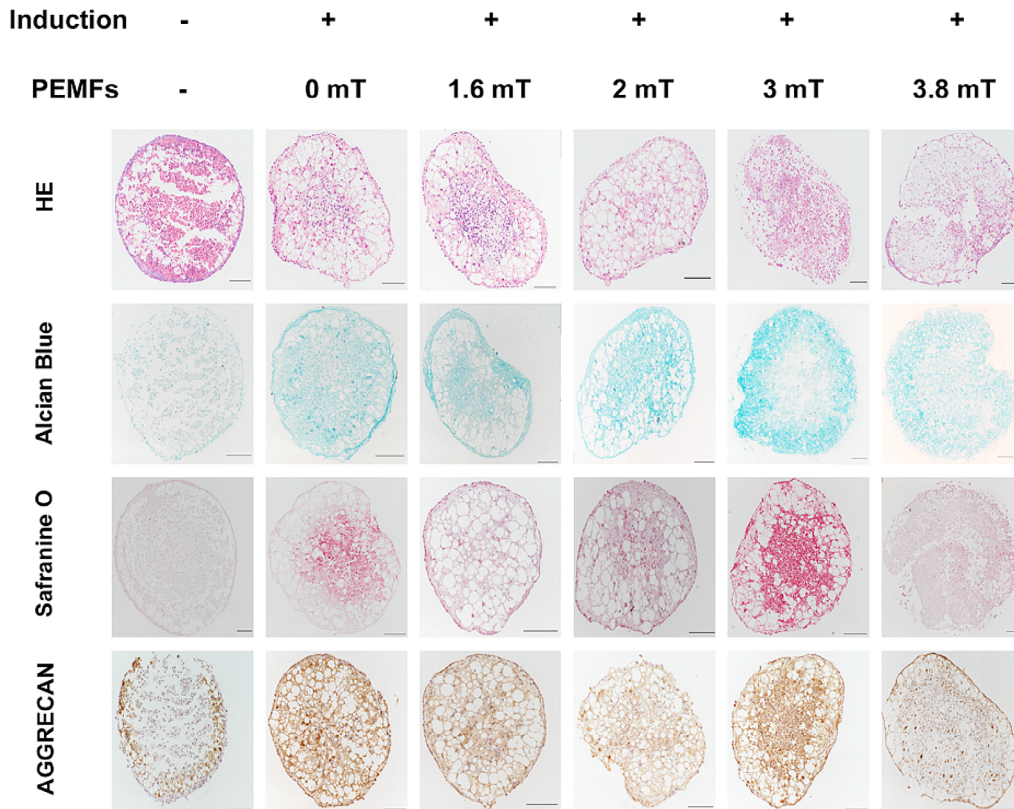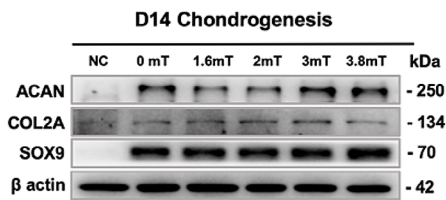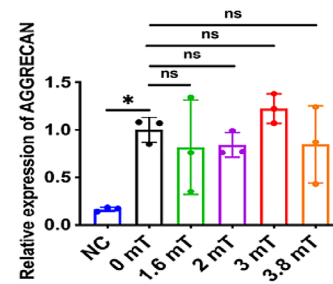
Fig. 2 3 mT PEMFs promoted chondrogenic differentiation of BMSCs in early stage of chondrogenesis. **(A)** Representative images of HE staining, Alcian blue and Safranine O for proteoglycan deposition in pellets derived from BMSCs and IHC for the expression of ACAN. Group with or without chondrogenic induction and PEMFs were indicated with black font in the top of each line of images. **(B)** The protein levels of ACAN, COL2A and SOX9 were investigated by western blotting. β-actin was used as baseline control. **(C)** Quantification of the relative expression level of ACAN. **(D)** Quantification of the relative expression level of COL2A. **(E)** Quantification of the relative expression level of SOX9. ns, $p>0.05$; * $p<0.05$; ** $p<0.01$; *** $p<0.001$. Student's t test and one-way ANOVA were used for comparison between two groups and multiple groups, respectively. Scale bar: 100 mm
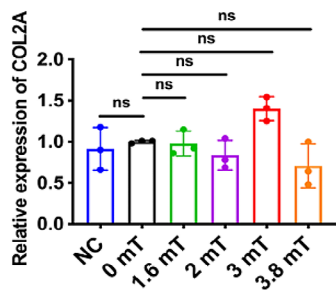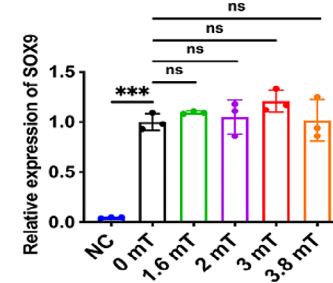
Fig. 3 3 mT PEMFs promoted chondrogenic differentiation of BMSCs in early stage of chondrogenesis. **(A)** Representative images of HE staining, Alcian blue and Safranine O for proteoglycan deposition in pellets derived from BMSCs and IHC for the expression of ACAN. Group with or without chondrogenic induction and PEMFs were indicated with black font in the top of each line of images. **(B)** The protein levels of ACAN, COL2A and SOX9 were investigated by western blotting. β-actin was used as baseline control. **(C)** Quantification of the relative expression level of ACAN. **(D)** Quantification of the relative expression level of COL2A. **(E)** Quantification of the relative expression level of SOX9. ns, $p > 0.05$; * $p < 0.05$; ** $p < 0.01$; *** $p < 0.001$. Student's t test and one-way ANOVA were used for comparison between two groups and multiple groups, respectively. Scale bar: 100 mm
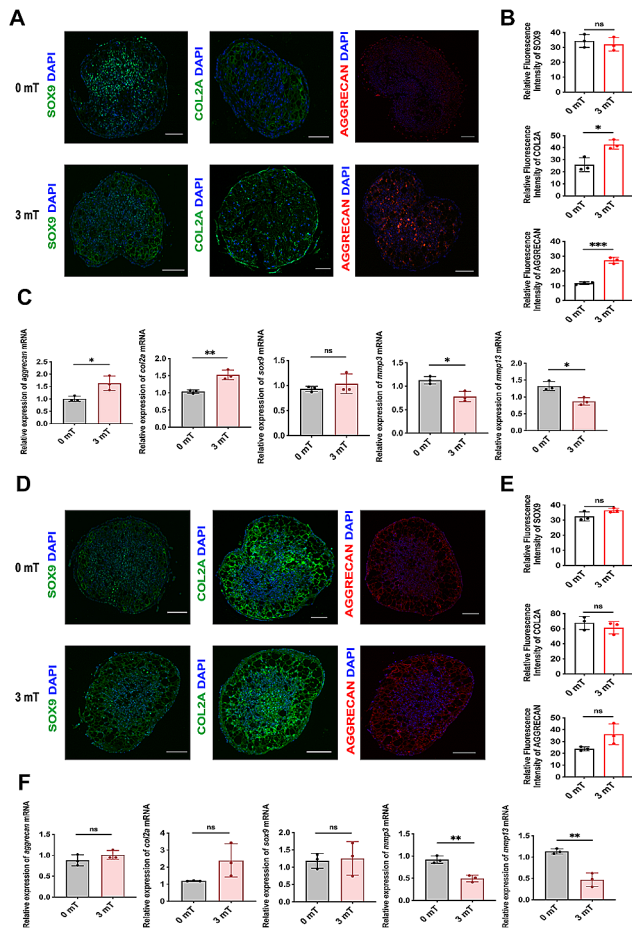
Fig. 4 3 mT PEMFs promoted chondrogenic differentiation of BMSCs in early stage of chondrogenesis. **(A)** Representative immunofluorescence images of ACAN (red), COL2A (green), SOX9 (green) and DAPI (blue) in both 0 mT and 3 mT groups of day 7 pellets. **(B)** Quantification of the fluorescence intensities for ACAN, COL2A and SOX9 of day 7 pellets. **(C)** Quantification of the transcript levels of *acan, col2a, sox9, mmp3* and mmp13 of day 7 pellets. **(D)** Representative immunofluorescence images of ACAN (red), COL2A (green), SOX9 (green) and DAPI (blue) in both 0 mT and 3 mT groups of day 14 pellets. **(E)** Quantification of the fluorescence intensities for ACAN, COL2A and SOX9 of day 14 pellets. **(F)** Quantification of the transcript levels of *acan, col2a, sox9, mmp3 and mmp13* of day 14 pellets. ns, $p>0.05$; * $p<0.05$; ** $p<0.01$; *** $p<0.001$. Student's t test and one-way ANOVA were used for comparison between two groups and multiple groups, respectively. Scale bar: 100 mm

sFRP3 expression at both timepoints (Fig. 5F - G). The discrepancy in β-catenin expression at the two timepoints provided a possible explanation for differences in cell morphology and chondrogenic-related factors on days 7 and 14, highlighting an early-stage chondrogenic protective impact of 3 mT PEMFs via the Wnt/β-catenin signaling pathway. Our findings collectively highlighted the role of frzb in promoting BMSCs chondrogenic differentiation during PEMF exposure, specifically influencing the Wnt/β-catenin signaling pathway.

3 mT PEMFs inhibit inflammation and promote chondrogenic differentiation of BMSCs in an inflammatory microenvironment

Inflammation constitutes a critical factor in the pathogenesis of KOA, exerting multifaceted influences on various cellular processes, including differentiation and homeostasis [41]. IL-1β was added to the medium to simulate an inflammatory microenvironment to assess how inflammation influences the potential of BMSCs for chondrogenesis with PEMFs treatment. On day 7, the 0 mT group showed considerably higher levels of p-p65 and p-STAT3, confirming the establishment of the inflammatory model. As expected, 3 mT PEMFs suppressed the levels of p-p65 and p-STAT3 on days 7 and 14 but had no effect on p65 or STAT3 (Fig. 6A-B). This suggests that 3 mT PEMFs reduced inflammation by reducing the phosphorylation and activation of inflammatory molecules.

Next, we assessed how PEMFs modulated chondrogenic differentiation in an inflammatory setting. Elevated levels of IL-1β suppressed chondrogenesis of MSCs by promoting catabolic activities and hastening cartilage degradation [12, 42]. Bur 3 mT PEMFs reversed the catabolic profile of inflammation by significantly downregulating MMP3 and MMP13 (Fig. 6A-B). In addition to limiting the catabolic activities induced by inflammation, PEMFs promoted BMSC anabolism by upregulating ACAN and COL2A (Fig. 7A-B), specifically reversing the IL-1β-induced suppression of ACAN from inflammation (Fig. 7A).

The Wnt/β-catenin signaling pathway is inhibited in the early phase of chondrogenesis within an inflammatory condition

The PEMFs treatment target gene *frzb*, which encodes sFRP3 and subsequently promotes BMSCs chondrogenic differentiation, was screened out. With additional IL-1β inhibition, the efficacy of this mechanism was unclear. Surprisingly, we still observed a significant upregulation of sFRP3 under inflammatory circumstances on days 7 and 14 (Fig. 8A - B). To confirm the activation of the Wnt/β-catenin signaling pathway, we examined the important downstream molecule β-catenin. and noticed a significant downregulation post 3 mT PEMF treatment on day 7 (Fig. 8A) but not on day 14 (Fig. 8B). It was stressed once more that PEMFs exhibit a chondroprotective impact in the early stages by suppressing Wnt/β-catenin signaling, even in an inflammatory context.

PEMFs inhibit the Wnt/β-catenin signaling pathway in vivo and protect articular cartilage

In vivo experiments were conducted to validate the identified parameters. DMM or sham surgery was performed on 10-week-old mice, followed by four weeks
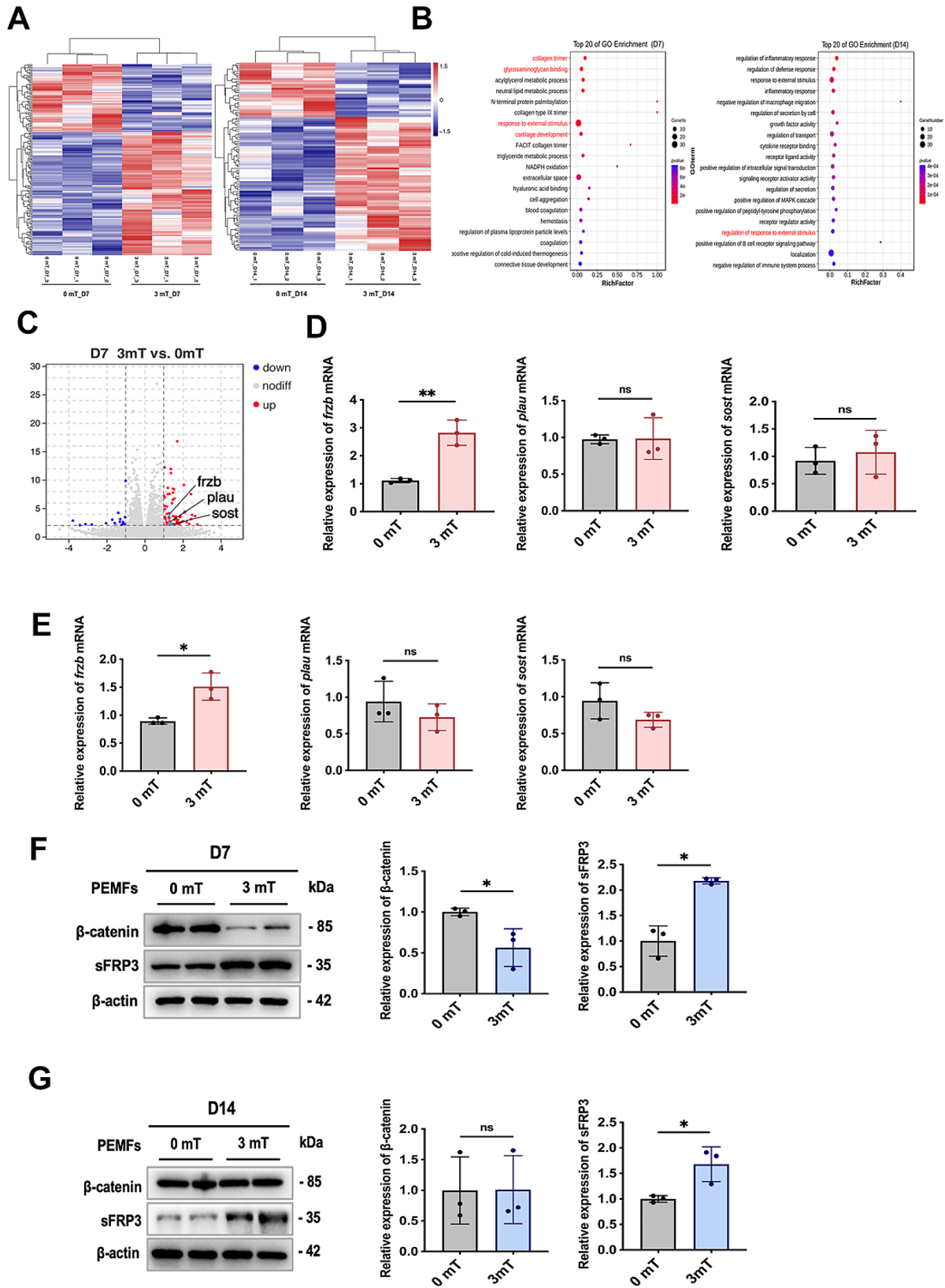
Fig. 5 (See legend on next page.)

(See figure on previous page.)

Fig. 5 *frzb* functioned during PEMFs exposure to enhance BMSCs chondrogenic differentiation and was related to Wnt-βcatenin signaling pathway. **(A)** Clustering heatmaps illustrated the expression levels of differential genes in day 7 and day 14 (n = 3). **(B)** Gene Ontology (GO) analysis of upregulated genes in pellets transcriptome (Top 20). **(C)** A volcano plot illustrated three targeted genes in the upregulated site (*frzb, plau, sost*). **(D)** Quantification of the transcript levels of *frzb, plau* and sost of day 7 pellets. **(E)** Quantification of the transcript levels of *frzb, plau* and *sost* of day 14 pellets. **(F)** For day 7 pellets, the protein levels of β-catenin and sFRP3 and quantification of the relative expression level of β-catenin and sFRP3. **(G)** For day 14 pellets, the protein levels of β-catenin and sFRP3 and quantification of the relative expression level of β-catenin and sFRP3. ns, $p > 0.05$; * $p < 0.05$; ** $p < 0.01$; *** $p < 0.001$. Student's t test and one-way ANOVA were used for comparison between two groups and multiple groups, respectively

of PEMFs exposure. The DMM group proved that the KOA model was successful by exhibiting severe cartilage degradation and a significant increase in OARSI score compared to the control group. However, PEMFs treatment significantly mitigated the increased OARSI score and cartilage loss in the PEMFs group compared to the DMM group, attenuating the DMM-induced OA lesions (Fig. 9B). In addition, IHC staining showed that PEMFs treatment (75 Hz, 3 mT, 1 h/d) resulted in protectively enhanced expression of ACAN and COL2A post-DMM. The expression of catabolic-related proteins (MMP3, MMP13, ADAMTS4) decreased noticeably simultaneously (Fig. 9C). As shown by the decreased expression of Wnt3a, β-catenin, and IL-1β in the IHC staining of the PEMFs group, PEMFs treatment prevented cartilage destruction and slowed the progression of inflammation. These findings showed that PEMFs exposure upregulated the expression of anabolic-related proteins and hindered the catabolic process, resulting in an in vivo cartilage-protective effect against OA, mostly through suppressing the Wnt/β-catenin signaling pathway coupled with inflammation.

Discussion

PEMFs are a noninvasive therapeutic approach with significant potential for enhancing regenerative processes in various musculoskeletal conditions by influencing several biological mechanisms. This study primarily examined the ability of PEMFs to promote the chondrogenic differentiation of BMSCs as a potential treatment for KOA. While previous studies explored how different PEMFs parameters affect BMSCs' differentiation into chondrocyte-like cells, the optimal intensity parameter had not yet been identified. Our findings were consistent with earlier studies, showing that exposure to PEMFs can facilitate BMSCs' chondrogenic differentiation [20, 24, 43, 44]. Our prior research indicated that 75 Hz was the optimal PEMFs frequency for BMSCs-based chondrogenic induction [19, 29, 34].

In this study, we further refined the electromagnetic efficacy window, revealing that 3 mT PEMFs had the optiaml influence on inducing chondrogenesis. However, another study using human ADSCs reported differing results, finding increased calcium deposition after 10 days of 15 Hz, 2 mT PEMFs therapy, even within a chondrogenic microenvironment [45]. These conflicting findings suggest that PEMFs interventions may have

diverse and complex biological effects. The discrepancies between our day 7 and day 14 results might help explain these variances in chondrogenesis and underscore the importance of optimal exposure duration. Our results demonstrated that the effectiveness of 3 mT PEMFs diminished over time, with reduced chondrogenic phenotypes observed after a 14-day exposure. This aligns with research indicating that 4 weeks of 75 Hz PEMFs therapy decreased the maintenance of the cartilaginous phenotype and exacerbated the breakdown of cartilage-specific extracellular matrix, regardless of intensity [28]. Thus, it is reasonable to conclude that both the parameters and duration of PEMFs treatment influence its efficacy window, with 3 mT PEMFs showing the greatest effect in the early stages of chondrogenic differentiation.

Regarding the anti-inflammatory effect of PEMFs therapy, we observed that PEMFs therapy reduced levels of TNF-α in rabbits with OA [29]. To replicate pathological OA conditions, we introduced the potent proinflammatory cytokine IL-1β into the culture medium. Our results showed that 3 mT PEMFs could reduce the expression of p-p65 and p-STAT3, both of which were elevated due to IL-1β treatment. The phosphorylation of p65 activates the NF-κB inflammatory pathway, triggering cellular behaviors such as matrix degradation and apoptosis. NF-κB/p-p65 also inhibits the chondrogenic process by suppressing the expression of sox9, a chondrogenic factor [46]. Our findings suggest that PEMFs might mitigate the effects of IL-1β on the NF-κB signaling pathway, thereby protecting chondrogenesis in BMSCs under inflammatory conditions. Specifically, 3 mT PEMFs reversed the IL-1β-induced downregulation of chondrogenic-related proteins, such as ACAN and COL2A, while reducing the overexpression of matrix metalloproteinases MMP3 and MMP13. These results align with findings by Ongaro et al. [25], which demonstrated that PEMFs counteract IL-1β-induced inhibition of proteoglycan synthesis and ACAN and COL2A mRNA expression during MSCs chondrogenesis induction. Collectively, these findings highlight the therapeutic potential of PEMFs in reducing inflammation progression and mitigating cartilage damage in knee osteoarthritis.

The Wnt/β-catenin pathway is a key therapeutic target for KOA treatment, playing a crucial role in development and tissue regeneration. Secreted Frizzled-related Proteins (sFRPs), antagonists of the Wnt/β-catenin pathway, have been shown to reverse cartilage degradation and
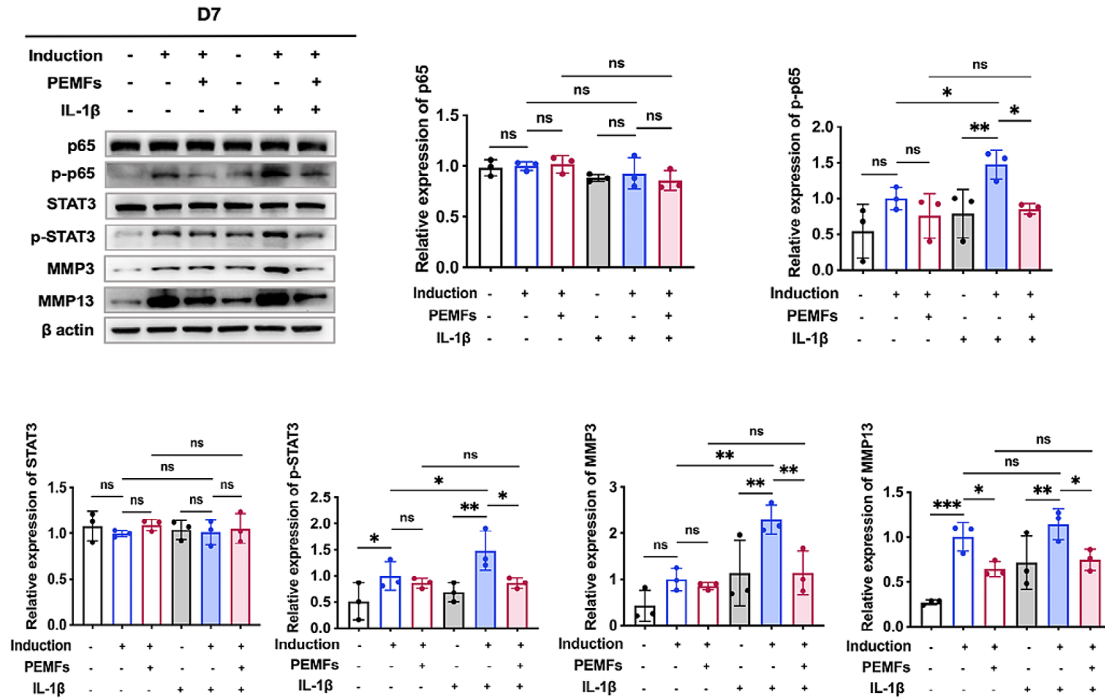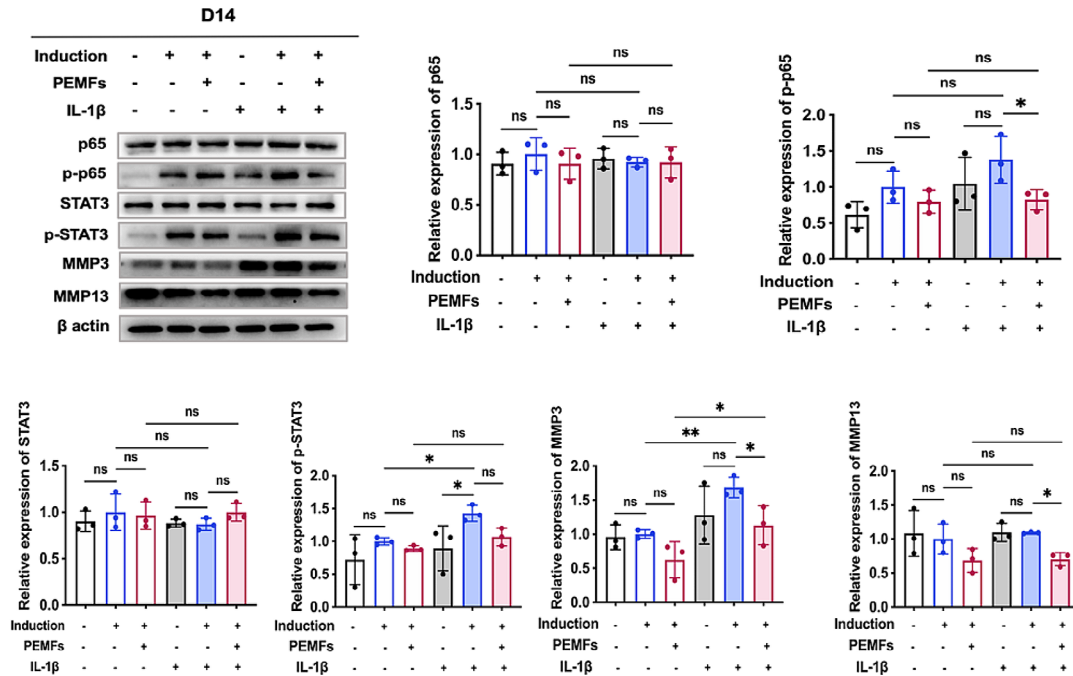
Fig. 6 3 mT PEMFs inhibited inflammation and promoted chondrogenic differentiation of BMSCs under inflammation condition. **(A)** For day 7 pellets: the protein levels of p65, p-p65, STAT3 and p-STAT3, which showed the level of inflammation, were investigated by western blotting. In addition, the catabolic-related proteins of chondrocytes (MMP3 and MMP13) were also displayed. Quantification of relative expression of these proteins were performed. **(B)** For day 14 pellets: the protein levels of the p65, p-p65, STAT3, p-STAT3, MMP3 and MMP13 and quantification of relative expression of these proteins. ns, $p > 0.05$; * $p < 0.05$; ** $p < 0.01$; *** $p < 0.001$. Student's t test and one-way ANOVA were used for comparison between two groups and multiple groups, respectively
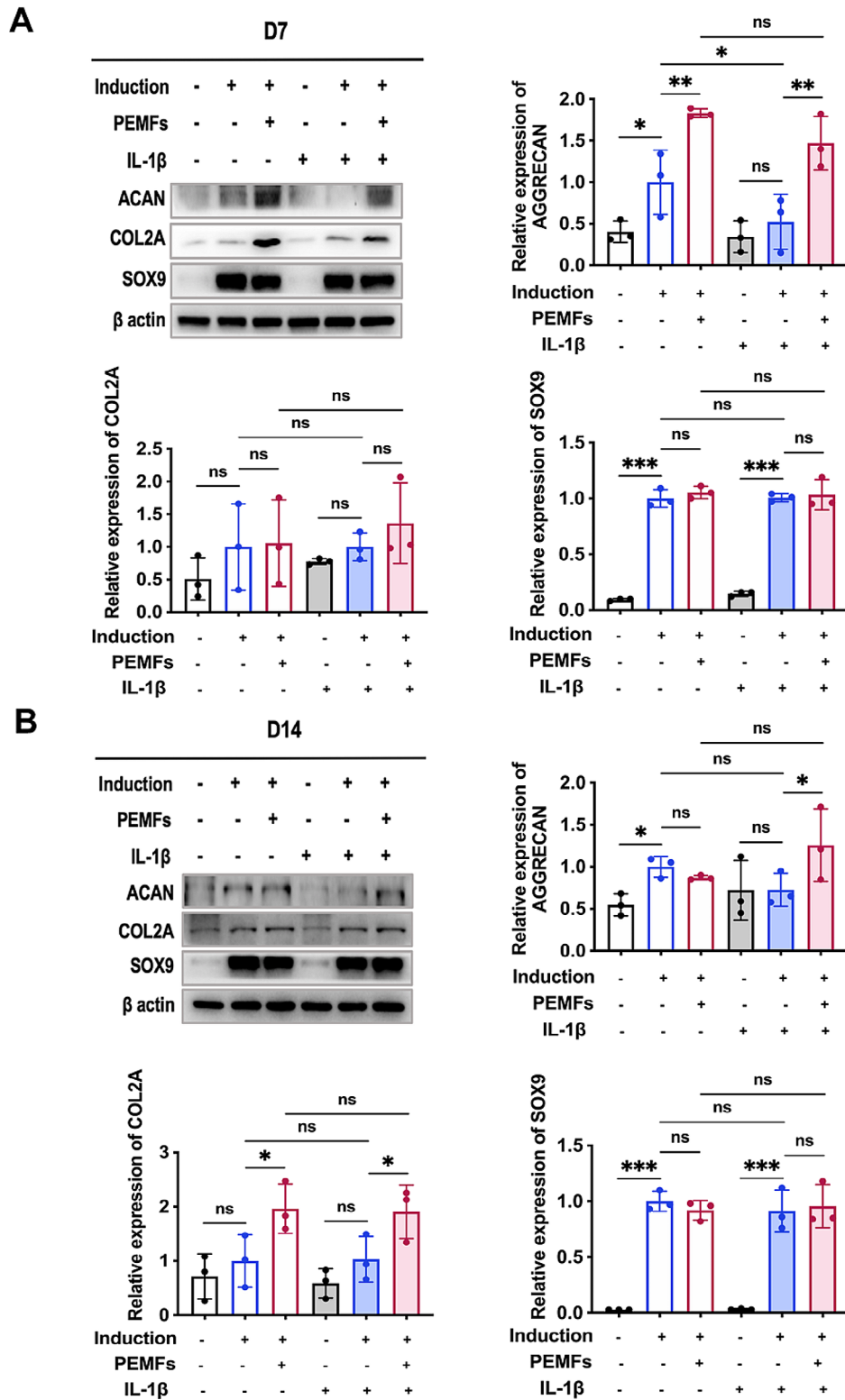
Fig. 7 3 mT PEMFs inhibited inflammation and promoted chondrogenic differentiation of BMSCs under inflammation condition. **(A)** For day 7 pellets, the protein levels of ACAN, COL2A and SOX9 were investigated by western blotting under inflammation condition. Quantification of the relative expression level of these proteins were performed. **(B)** For day 14 pellets, the protein levels of ACAN, COL2A and SOX9 were displayed, and quantification of relative expression of these proteins. ns, $p > 0.05$; * $p < 0.05$; ** $p < 0.01$; *** $p < 0.001$. Student's t test and one-way ANOVA were used for comparison between two groups and multiple groups, respectively
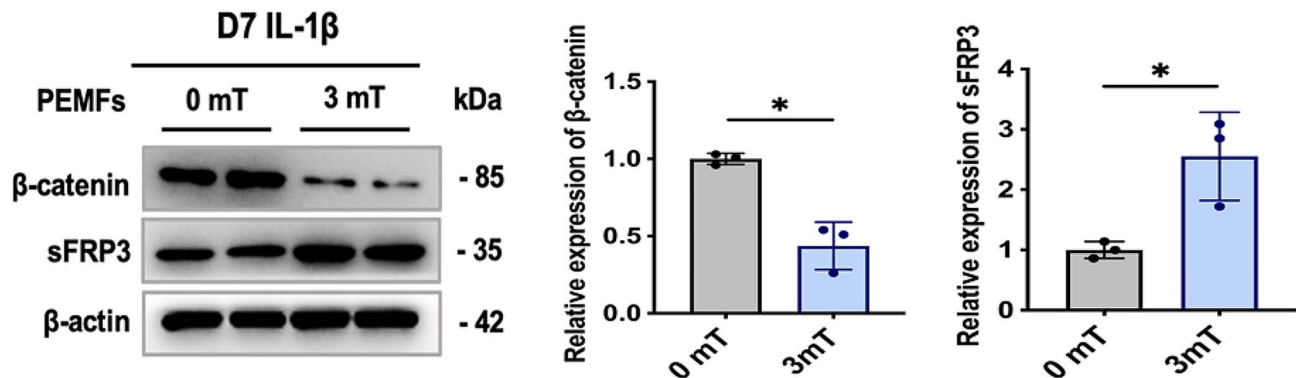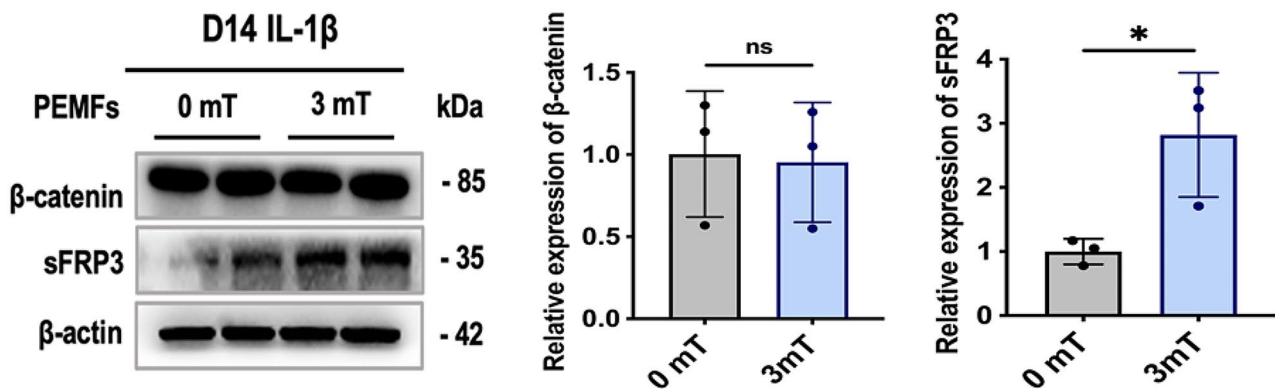
Fig. 8 Wnt-βcatenin signaling pathway were inhibited in the early stage of chondrogenesis under inflammation condition. **(A)** For day 7 pellets, the protein levels of β-catenin and sFRP3 were investigated by western blotting. Quantification of the relative expression level of these two proteins were performed. **(B)** For day 14 pellets, the protein levels of β-catenin and sFRP3 were displayed, and quantification of relative expression of these two proteins. ns, $p>0.05$; * $p<0.05$; ** $p<0.01$; *** $p<0.001$. Student's t test and one-way ANOVA were used for comparison between two groups and multiple groups, respectively

inhibit the chondrogenic effects induced by this pathway [47]. In our study, we found that 3 mT PEMFs enhanced the chondrogenesis of BMSCs by influencing sFRPs and inhibiting the Wnt/β-catenin pathway. Notably, the gene frzb, which encodes sFRPs, is typically downregulated in KOA [48] but was consistently upregulated following exposure to 3 mT PEMFs, correlating with a protective effect on cartilage. This finding underscores the potential of frzb as a therapeutic target for addressing cartilage dysregulation in KOA. The chondroprotective effect of inhibiting the Wnt/β-catenin pathway through frzb upregulation has been confirmed. Xu et al. [49] previously demonstrated that exogenous FRZB effectively suppressed the Wnt/β-catenin pathway by downregulating β-catenin, Wnt3A, and Wnt8A, leading to an upregulation of chondrogenic markers such as SOX9, ACAN, and COL2A, while also inhibiting the catabolic activities and osteogenesis of BMSCs. In our current study,

we identified for the first time that frzb and the Wnt/β-catenin pathway are key targets for PEMFs intervention in the chondrogenic differentiation of BMSCs. Additionally, PEMFs not only reduced inflammation but also altered the Wnt/β-catenin pathway to enhance chondrogenic differentiation under inflammatory conditions.

However, we observed that β-catenin, the downstream molecule of the canonical Wnt/β-catenin pathway, did not exhibit expression levels corresponding to the upregulation of frzb across the two evaluation time points. This suggests the potential involvement of other molecules or crosstalk with alternative signaling pathways. Inflammation is intricately linked with the Wnt/β-catenin pathway, and the interaction between the Wnt/β-catenin and NF-κB pathways is complex. For instance, NF-κB and STAT3-mediated inhibition of the Wnt/β-catenin pathway has shown a cartilage regenerative effect in animal models [50]. Conversely, Ma et al. found that Wnt3A
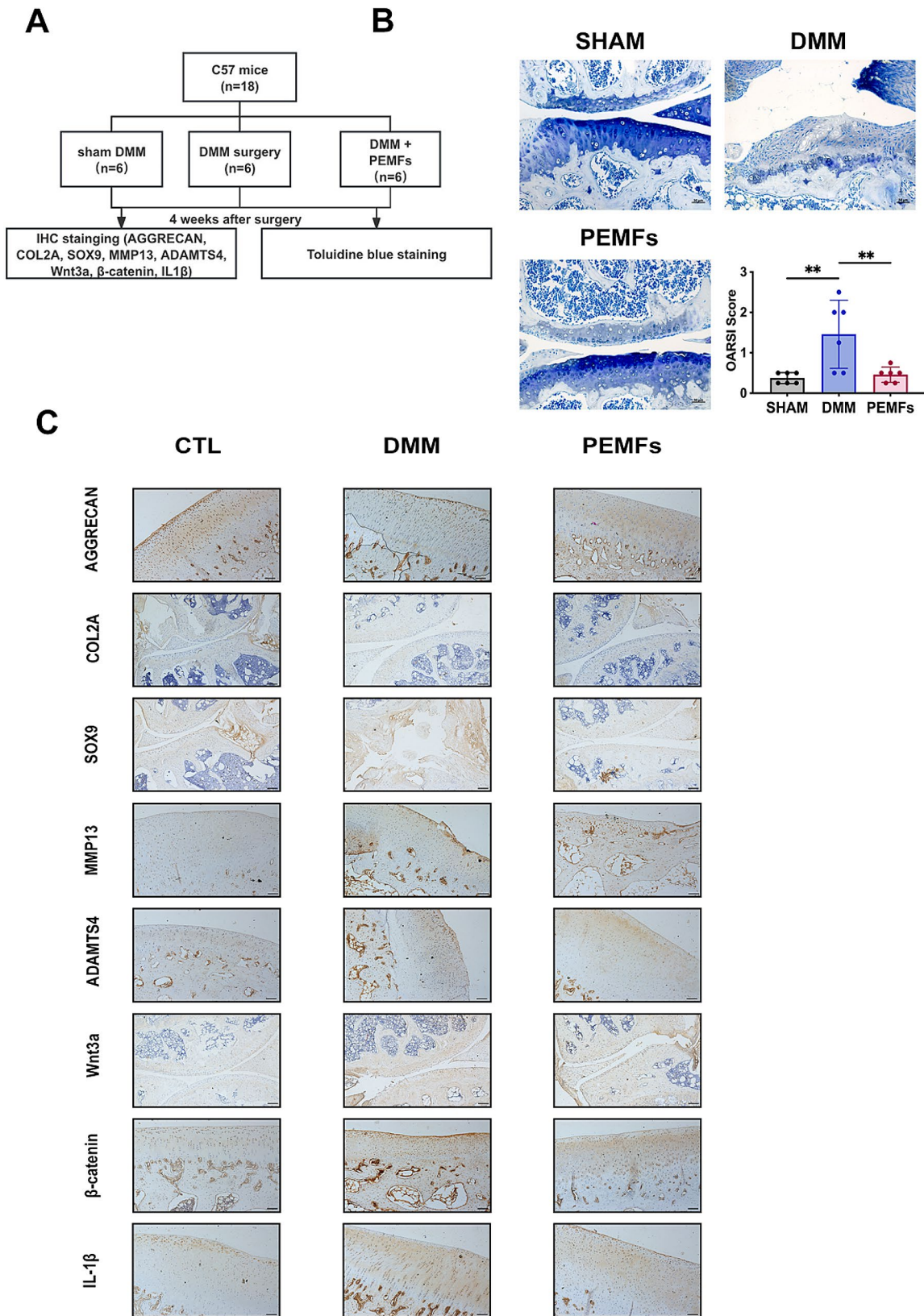
Fig. 9 PEMFs exerted cartilage protection effect in DMM induced OA model and inhibited Wnt-βcatenin signaling pathway in vivo. **(A)** Schematic of the in vivo group set. **(B)** Representative Toluidine Blue-stained joint sections from mice post sham-DMM surgery, DMM surgery, DMM surgery and PEMFs treatment and quantification of OARSI scores. Scale bar: 100 mm. **(C)** Representative immunohistochemical staining of ACAN, COL2A, SOX9, MMP13, ADAMTS4, Wnt3a, β-catenin and IL-1β (n = 3). Scale bar: 100 mm

inhibited NF-κB signaling, resulting in an unexpected anticatabolic effect [51]. Further studies are required to explore the intrinsic mechanisms of PEMFs-modulated interactions between the Wnt/β-catenin and NF-κB pathways and their impact on BMSCs chondrogenesis, which might be crucial for maintaining cartilage integrity in an inflammatory microenvironment.

PEMFs are widely recognized for their therapeutic potential in treating skeletal system disorders [52, 53] and have generated significant interest in regenerative medicine [54, 55]. Our study focused on determining the optimal PEMF parameters for inducing chondrogenic differentiation in BMSCs, thus filling a knowledge gap regarding early-phase BMSC responses to these parameters in the context of chondrogenesis. We identified the key molecular targets, frzb, and the primary Wnt/β-catenin pathway through which PEMFs exert their therapeutic effects. Integrating PEMFs with tissue engineering allows for localized treatment targeting KOA, which avoids the adverse effects associated with global immunosuppression [56]. These findings suggest a promising strategy for addressing cartilage damage in degenerative joint diseases like KOA. Nevertheless, the complexity of the Wnt/β-catenin signaling pathway, which involves numerous molecules, requires further in-depth investigation.

Conclusion
This study establishes the optimal parameters for PEMF treatment: a 3 mT intensity in square waveform, 75 Hz frequency, and a daily exposure duration of 1 h. These parameters are identified as potent stimulators that effectively promote the chondrogenic differentiation of BMSCs, particularly during the early phase of chondrogenesis. Furthermore, our investigation highlights the critical role of sFRP3 in responding to PEMF treatment. sFRP3 modulates the Wnt/β-catenin signaling cascade, thereby enhancing chondrogenesis. Additionally, our findings extend to an inflammatory microenvironment, demonstrating that PEMFs can reverse inflammation and promote chondrogenesis by regulating sFRP3 and the Wnt/β-catenin signaling pathway.

Clinical perspectives
Background
This study explored the efficacy of Pulsed Electromagnetic Fields (PEMFs) in treating knee osteoarthritis (KOA). Specifically, it aimed to induce chondrogenic differentiation in Bone Marrow-Derived Mesenchymal Stem Cells (BMSCs) and elucidate the underlying cellular mechanisms.

Results
BMSCs exposed to 3mT PEMFs at 75 Hz demonstrated optimal chondrogenic differentiation at 7 days. This was characterized by the upregulation of chondrogenic markers such as ACAN, COL2A, and SOX9, alongside the downregulation of matrix-degrading enzymes like MMP3 and MMP13. Transcriptome analysis identified sFRP3 as a pivotal mediator, which inhibits the Wnt/β-catenin signaling pathway regardless of inflammatory conditions.

Significance
These findings suggest that PEMFs therapy could significantly contribute to KOA treatment by promoting cartilage repair and mitigating degeneration. A deeper understanding of these regulatory mechanisms could facilitate targeted interventions, offering hope for improved management of KOA and potentially other musculoskeletal disorders.

Abbreviations
OA	Osteoarthritis
KOA	Knee Osteoarthritis
BMSCs	Bone Bone Marrow-Derived Mesenchymal Stem Cells
PEMFs	Pulsed Electromagnetic Fields

Supplementary Information
The online version contains supplementary material available at https://doi.org/10.1186/s12967-024-05470-7.

Supplementary Material 1

Data availability
The dataset supporting the conclusions of this article is available in the GSA database, under project PRJCA020963 and accession number CRA013278. Supplementary material associated with this paper can be found in Supplemental materials.docx.

Declarations

Ethical approval
The in vivo study adhered to the ARRIVE guidelines (Version 2.0) [30]. All experimental procedures were approved by the Institutional Animal Care and Use Committee of West China Hospital, Sichuan University (IACUC permit number 20220224091, approved on February 28, 2022).

Consent for publication
Not applicable.

Competing interests
The authors declare that they have no competing interests.

Author details
¹Rehabilitation Medicine Center, Institute of Rehabilitation Medicine, West China Hospital, Sichuan University, #37 Guoxue Alley, Wuhou strict, Chengdu, Sichuan 610041, PR China
²Key Laboratory of Rehabilitation Medicine in Sichuan Province, West China Hospital, Sichuan University, Chengdu, China
³School of Rehabilitation Sciences, West China School of Medicine, Sichuan University, Chengdu, China
⁴The Lab of Aging Research, State Key Laboratory of Biotherapy, West China Hospital, National Clinical Research Center for Geriatrics, Sichuan University, Chengdu, China

References
1. Bannuru RR, Osani M, Vaysbrot E, Arden N, Bennell K, Bierma-Zeinstra S, et al. OARSI guidelines for the non-surgical management of knee, hip, and polyarticular osteoarthritis. Osteoarthr Cartil. 2019;27(11):1578–89.
2. Association JSBotCO. Chinese guideline for diagnosis and treatment of osteoarthritis (2021 edition). Chin J Orthop. 2021;41(18):1291–314.
3. Long H, Liu Q, Yin H, Wang K, Diao N, Zhang Y, et al. Prevalence trends of site-specific osteoarthritis from 1990 to 2019: findings from the global burden of Disease Study 2019. Arthritis Rheumatol. 2022;74(7):1172–83.
4. Yang G, Wang J, Liu Y, Lu H, He L, Ma C, et al. Burden of knee osteoarthritis in 204 countries and territories, 1990–2019: results from the global burden of Disease Study 2019. ARTHRIT CARE RES. 2023;75(12):2489–500.
5. Xiang X-N, Zhu S-Y, He H-C, Yu X, Xu Y, He C-Q. Mesenchymal stromal cell-based therapy for cartilage regeneration in knee osteoarthritis. Stem Cell Res Ther. 2022;13:1–20.
6. Zhu S, Wang Z, Liang Q, Zhang Y, Li S, Yang L, et al. Chinese guidelines for the rehabilitation treatment of knee osteoarthritis: an CSPMR evidence-based practice guideline. J Evidence-Based Med. 2023;16(3):376–93.
7. Kolasinski SL, Neogi T, Hochberg MC, Oatis C, Guyatt G, Block J, et al. 2019 American College of Rheumatology/Arthritis Foundation guideline for the management of osteoarthritis of the hand, hip, and knee. ARTHRITIS RHEUMATOL. 2020;72(2):220–33.
8. Cho Y, Jeong S, Kim H, Kang D, Lee J, Kang S-B, et al. Disease-modifying therapeutic strategies in osteoarthritis: current status and future directions. Exp Mol Med. 2021;53(11):1689–96.
9. Ding N, Li E, Ouyang X, Guo J, Wei B. The therapeutic potential of bone marrow mesenchymal stem cells for articular cartilage regeneration in Osteoarthritis. Curr Stem Cell Res Ther. 2021;16(7):840–7.
10. Lee E, Epanomeritakis IE, Lu V, Khan W. Bone marrow-derived mesenchymal stem cell implants for the treatment of focal Chondral defects of the knee in animal models: a systematic review and Meta-analysis. Int J Mol Sci. 2023;24(4).
11. Soler R, Orozco L, Munar A, Huguet M, Lopez R, Vives J, et al. Final results of a phase I-II trial using ex vivo expanded autologous mesenchymal stromal cells for the treatment of osteoarthritis of the knee confirming safety and suggesting cartilage regeneration. Knee. 2016;23(4):647–54.
12. Wang Z, He Z, Zhang W, Liang S, Chen K, Xu S, et al. Glycogen synthase kinase 3beta inhibits BMSCs chondrogenesis in inflammation via the cross-reaction between NF-kappaB and beta-catenin in the Nucleus. Stem Cells Int. 2022;2022:5670403.
13. Chen C, Bao GF, Xu G, Sun Y, Cui ZM. Altered wnt and NF-kappaB signaling in Facet Joint Osteoarthritis: insights from RNA deep sequencing. Tohoku J Exp Med. 2018;245(1):69–77.
14. Jridi I, Cante-Barrett K, Pike-Overzet K, Staal FJT. Inflammation and wnt signaling: target for Immunomodulatory Therapy? Front Cell Dev Biol. 2020;8:615131.
15. Marsh S, Constantin-Teodosiu T, Chapman V, Sottile V. In vitro exposure to Inflammatory Mediators affects the differentiation of mesenchymal progenitors. Front Bioeng Biotechnol. 2022;10:908507.
16. Wehling N, Palmer GD, Pilapil C, Liu F, Wells JW, Muller PE, et al. Interleukin-1beta and tumor necrosis factor alpha inhibit chondrogenesis by human mesenchymal stem cells through NF-kappaB-dependent pathways. Arthritis Rheum. 2009;60(3):801–12.
17. Zhong L, Schivo S, Huang X, Leijten J, Karperien M, Post JN. Nitric oxide mediates crosstalk between Interleukin 1beta and WNT signaling in primary human chondrocytes by reducing DKK1 and FRZB expression. Int J Mol Sci. 2017;18(11).
18. Yang X, He H, Ye W, Perry TA, He C. Effects of Pulsed Electromagnetic Field Therapy on Pain, stiffness, physical function, and quality of life in patients with osteoarthritis: a systematic review and Meta-analysis of Randomized Placebo-controlled trials. Phys Ther. 2020;100(7):1118–31.
19. Yang X, He H, Zhou Y, Zhou Y, Gao Q, Wang P, et al. Pulsed electromagnetic field at different stages of knee osteoarthritis in rats induced by low-dose monosodium iodoacetate: Effect on subchondral trabecular bone microarchitecture and cartilage degradation. Bioelectromagnetics. 2017;38(3):227–38.
20. Veronesi F, Fini M, Giavaresi G, Ongaro A, De Mattei M, Pellati A, et al. Experimentally induced cartilage degeneration treated by pulsed electromagnetic field stimulation; an in vitro study on bovine cartilage. BMC Musculoskelet Disord. 2015;16:308.
21. Ongaro A, Pellati A, Masieri FF, Caruso A, Setti S, Cadossi R, et al. Chondroprotective effects of pulsed electromagnetic fields on human cartilage explants. Bioelectromagnetics. 2011;32(7):543–51.
22. Varani K, Vincenzi F, Ravani A, Pasquini S, Merighi S, Gessi S, et al. Adenosine Receptors as a Biological pathway for the anti-inflammatory and beneficial effects of low frequency Low Energy Pulsed Electromagnetic fields. Mediators Inflamm. 2017;2017:2740963.
23. Varani K, Vincenzi F, Pasquini S, Blo I, Salati S, Cadossi M et al. Pulsed Electromagnetic Field Stimulation in Osteogenesis and Chondrogenesis: signaling pathways and therapeutic implications. Int J Mol Sci. 2021;22(2).
24. Esposito M, Lucariello A, Costanzo C, Fiumarella A, Giannini A, Riccardi G, et al. Differentiation of human umbilical cord-derived mesenchymal stem cells, WJ-MSCs, into chondrogenic cells in the presence of pulsed electromagnetic fields. Vivo. 2013;27(4):495–500.
25. Ongaro A, Pellati A, Setti S, Masieri FF, Aquila G, Fini M, et al. Electromagnetic fields counteract IL-1beta activity during chondrogenesis of bovine mesenchymal stem cells. J Tissue Eng Regen Med. 2015;9(12):E229–38.
26. Parate D, Franco-Obregon A, Frohlich J, Beyer C, Abbas AA, Kamarul T, et al. Enhancement of mesenchymal stem cell chondrogenesis with short-term low intensity pulsed electromagnetic fields. Sci Rep. 2017;7(1):9421.
27. Kavand H, Haghighipour N, Zeynali B, Seyedjafari E, Abdemami B. Extremely low frequency Electromagnetic Field in Mesenchymal Stem cells Gene Regulation: chondrogenic markers evaluation. Artif Organs. 2016;40(10):929–37.
28. Wang J, Tang N, Xiao Q, Zhang L, Li Y, Li J, et al. Pulsed electromagnetic field may accelerate in vitro endochondral ossification. Bioelectromagnetics. 2015;36(1):35–44.
29. Yang X, Guo H, Ye W, Yang L, He C. Pulsed Electromagnetic Field attenuates Osteoarthritis Progression in a murine destabilization-Induced Model through Inhibition of TNF-alpha and IL-6 signaling. Cartilage. 2021;13(2suppl):S1665–75.
30. Percie du Sert N, Hurst V, Ahluwalia A, Alam S, Avey MT, Baker M, et al. The ARRIVE guidelines 2.0: updated guidelines for reporting animal research. J Cereb Blood Flow Metabolism. 2020;40(9):1769–77.
31. Huang L, Sun X, Wang L, Pei G, Wang Y, Zhang Q, et al. Enhanced effect of combining bone marrow mesenchymal stem cells (BMMSCs) and pulsed electromagnetic fields (PEMF) to promote recovery after spinal cord injury in mice. MedComm. 2022;3(3):e160.
32. Soleimani M, Nadri S. A protocol for isolation and culture of mesenchymal stem cells from mouse bone marrow. Nat Protoc. 2009;4(1):102–6.
33. Ramos L, Sánchez-Abarca T, Muntión LI, Preciado S, Puig S, López-Ruano N. MSC surface markers (CD44, CD73, and CD90) can identify human

MSC-derived extracellular vesicles by conventional flow cytometry. Cell Communication Signal. 2016;14:1–14.

34. Ye W, Guo H, Yang X, Yang L, He C. Pulsed Electromagnetic Field Versus whole body vibration on cartilage and subchondral trabecular bone in mice with knee osteoarthritis. Bioelectromagnetics. 2020;41(4):298–307.

35. Yang X, He H, Gao Q, He C. Pulsed electromagnetic field improves subchondral bone microstructure in knee osteoarthritis rats through a Wnt/beta-catenin signaling-associated mechanism. Bioelectromagnetics. 2018;39(2):89–97.

36. Ella-Tongwiis P, Makanga A, Shergill I, Hughes SF. Optimisation and validation of immunohistochemistry protocols for cancer research. Histol Histopathol. 2021;36(4):415–24.

37. Hofman FM, Taylor CR, Immunohistochemistry. Curr Protocols Immunol. 2013;103(1):21. 1-4. 6.

38. Gallagher S, Chakavarti D. Immunoblot analysis. JoVE (Journal Visualized Experiments). 2008;16:e759.

39. Kurien BT, Scofield RH. Western blotting. Methods. 2006;38(4):283–93.

40. Festing MF. Design and statistical methods in studies using animal models of development. ILAR J. 2006;47(1):5–14.

41. Goldring MB, Otero M. Inflammation in osteoarthritis. Curr Opin Rheumatol. 2011;23(5):471–8.

42. Haseeb A, Haqqi TM. Immunopathogenesis of osteoarthritis. Clin Immunol. 2013;146(3):185–96.

43. Mayer-Wagner S, Passberger A, Sievers B, Aigner J, Summer B, Schiergens TS, et al. Effects of low frequency electromagnetic fields on the chondrogenic differentiation of human mesenchymal stem cells. Bioelectromagnetics. 2011;32(4):283–90.

44. Parate D, Kadir ND, Celik C, Lee EH, Hui JHP, Franco-Obregon A, et al. Pulsed electromagnetic fields potentiate the paracrine function of mesenchymal stem cells for cartilage regeneration. Stem Cell Res Ther. 2020;11(1):46.

45. Chen CH, Lin YS, Fu YC, Wang CK, Wu SC, Wang GJ, et al. Electromagnetic fields enhance chondrogenesis of human adipose-derived stem cells in a chondrogenic microenvironment in vitro. J Appl Physiol (1985). 2013;114(5):647–55.

46. Murakami S, Lefebvre V, de Crombrugghe B. Potent inhibition of the master chondrogenic factor Sox9 gene by interleukin-1 and tumor necrosis factor-alpha. J Biol Chem. 2000;275(5):3687–92.

47. Zhong L, Huang X, Rodrigues ED, Leijten JC, Verrips T, El Khattabi M, et al. Endogenous DKK1 and FRZB regulate Chondrogenesis and Hypertrophy in three-dimensional cultures of human chondrocytes and human mesenchymal stem cells. Stem Cells Dev. 2016;25(23):1808–17.

48. Zhong L, Huang X, Karperien M, Post JN. Correlation between Gene expression and osteoarthritis progression in human. Int J Mol Sci. 2016;17(7).

49. Xu R, Zhang F, Lu J, Wang K, Pan P, Sun Y, et al. Secreted frizzled-related protein 3 was genetically and functionally associated with developmental dysplasia of the hip. Aging. 2021;13(8):11281–95.

50. Deshmukh V, O'Green AL, Bossard C, Seo T, Lamangan L, Ibanez M, et al. Modulation of the wnt pathway through inhibition of CLK2 and DYRK1A by lorecivivint as a novel, potentially disease-modifying approach for knee osteoarthritis treatment. Osteoarthritis Cartilage. 2019;27(9):1347–60.

51. Ma B, van Blitterswijk CA, Karperien M. A Wnt/β-catenin negative feedback loop inhibits interleukin-1–induced matrix metalloproteinase expression in human articular chondrocytes. Arthr Rheum. 2012;64(8):2589–600.

52. Cadossi R, Massari L, Racine-Avila J, Aaron RK. Pulsed Electromagnetic Field Stimulation of Bone Healing and Joint Preservation: Cellular mechanisms of skeletal response. J Am Acad Orthop Surg Glob Res Rev. 2020;4(5):e1900155.

53. Flatscher J, Pavez Lorie E, Mittermayr R, Meznik P, Slezak P, Redl H et al. Pulsed Electromagnetic fields (PEMF)-Physiological response and its potential in Trauma Treatment. Int J Mol Sci. 2023;24(14).

54. Ross CL, Ang DC, Almeida-Porada G. Targeting mesenchymal stromal Cells/Pericytes (MSCs) with pulsed electromagnetic field (PEMF) has the potential to treat rheumatoid arthritis. Front Immunol. 2019;10:266.

55. Iwasa K, Reddi AH. Pulsed Electromagnetic fields and tissue Engineering of the joints. Tissue Eng Part B Rev. 2018;24(2):144–54.

56. Ohtani S, Ushiyama A, Maeda M, Ogasawara Y, Wang J, Kunugita N, et al. The effects of radio-frequency electromagnetic fields on T cell function during development. J Radiat Res. 2015;56(3):467–74.

Publisher's Note